coatings

MDPI

Article

# Linear and Nonlinear Absorption of Titanium Dioxide Films Produced by Plasma Ion-Assisted Electron Beam Evaporation: Modeling and Experiments

**Olaf Stenzel [1,*], Steffen Wilbrandt [1], Christian Mühlig [2] and Sven Schröder [1]**

[1] Fraunhofer Institute of Applied Optics and Precision Engineering, IOF, Albert-Einstein-Str. 7, 07745 Jena, Germany; steffen.wilbrandt@iof.fraunhofer.de (S.W.); sven.schroeder@iof.fraunhofer.de (S.S.)

[2] Leibniz Institute of Photonic Technology, Albert-Einstein-Str. 9, 07745 Jena, Germany; christian.muehlig@leibniz-ipht.de

* Correspondence: olaf.stenzel@iof.fraunhofer.de; Tel.: +49-3641-807-348

Received: 20 December 2019; Accepted: 7 January 2020; Published: 9 January 2020


**Abstract:** Titanium dioxide films were prepared by plasma ion-assisted electron beam evaporation. Linear optical properties were investigated in terms of spectrophotometry using the beta-distributed oscillator (ß_do) model as a parametrized dispersion law. The nonlinear two-photon absorption coefficient of titanium dioxide was determined by means of the laser-induced deflection technique at a wavelength of 800 nm. The obtained values of (2–5) × $10^{-11}$ cm/W were consistent with published experimental values for rutile as well as for simulations performed in the frames of the ß_do and Sheik–Bahae models.

**Keywords:** optical coatings; titanium dioxide; optical constants; two-photon absorption; nonlinear refraction; scattering; laser-induced deflection; absorption measurement

## 1. Introduction

The standard theoretical apparatus used for modeling the optical properties of multilayer systems is formulated in terms of linear optics, i.e., it is based on a linear relationship between the electric field strength and the polarization induced in the medium. Within this framework, commonly used calculation recipes, such as matrix formalism or the admittance approach, have been derived in relevant textbooks [1–4]. Practical applications for these approaches in optical coatings design, characterization, and reengineering tasks have formed the content of relevant monographs (see, for example, References [2–5]).

Nevertheless, in high-power laser systems, the electric field in the incident light beam may be strong enough to induce relevant nonlinear optical effects in the coating materials. In many cases, it is the third-order (cubic) optical nonlinearity that dominates the nonlinear response. The optical Kerr effect, as well as nonlinear two-photon absorption (TPA), are prominent examples of third-order processes [6].

In high-power laser applications, third-order nonlinearity may therefore have to be taken into account in order to correctly predict the optical properties of a coating [7]. Thus, Razskazovskaya et al. [8] demonstrated the effect of TPA on the reflectance of dielectric laser mirrors in a pre-damage regime. Similarly, the optical Kerr effect appeared to be responsible for an intensity-dependent shift of the rejection band edge in several Angstroms in edge filters [9]. As opposed to linear optics, the general effect is that coating reflectance (and transmittance) becomes intensity-dependent. As we have shown in a previous study, these effects can principally be incorporated into a manageable design algorithm [10]

when describing each coating material by four (instead of two) optical constants, namely linear and nonlinear refractive indexes as well as linear and nonlinear extinction or absorption coefficients. Concerning linear optical constants, an overwhelming number of studies exist that give an idea on the range of optical constants achievable for practically any relevant coating material depending on the deposition technique and parameters used. However, although there exist several manageable theoretical approaches for estimating nonlinear optical constants (see, for example, References [11–16]), reliable experimental data on the dispersion of nonlinear optical constants of thin-film materials are practically not available.

The motivation of this study was to contribute to an improvement of the data basis for nonlinear optical constants. We present results from the measurement of the two-photon absorption coefficient of $TiO_2$ thin optical films at a wavelength of 800 nm and discuss the results with respect to the predictions of two different theoretical approaches.

## 2. Theoretical Background

Both nonlinear refraction and absorption may be (in terms of the lowest order with respect to the field strength) expressed in terms of the cubic nonlinear dielectric susceptibility $\chi^{(3)}$. General quantum-mechanical expressions for $\chi^{(3)}$ are available in relevant textbooks (compare Reference [6]), but because of the high number of input parameters, their direct usage may be inconvenient in practical applications. Instead, we will make use of simplified expressions that allow for estimating the TPA coefficient $\beta$ in terms of input parameters that are available from standard (linear) optical thin-film characterization techniques, among them spectrophotometry and ellipsometry.

In this context, the model of Sheik–Bahae et al. [15] provides a simple formula for calculating TPA contributions to nonlinear absorption in semiconducting solids. The material-specific input parameters of the model are the band gap $E_g$ as well as the usual linear refractive index $n$. Both these values may be obtained from linear optical spectroscopy. When choosing the remaining, rather material-independent model parameters corresponding to what is recommended in Reference [15], the expression for $\beta$ may be written as

$$\beta(\nu) \approx \frac{3100\sqrt{21}}{2^5 n^2 E_g^3} \frac{\left(\frac{2hc\nu}{E_g} - 1\right)^{\frac{3}{2}}}{\left(\frac{2hc\nu}{E_g}\right)^5}. \quad (1)$$

Equation (1) yields $\beta$ directly in cm/GW, provided that both $hc\nu$ and $E_g$ are given in eV (in which $h$ represents Planck's constant, $c$ is the velocity of light in a vacuum, and $\nu$ is the wavenumber, i.e., the reciprocal value of the light wavelength in a vacuum. In order to better understand the parametrization, Figure 1 shows estimated $\beta$ values corresponding to Equation (1) for the crystalline $TiO_2$ modifications of anatase, rutile, and brookite. The underlying parameters are summarized in Table 1. The crystal refractive indices indicated in Table 1 are polarization-averaged.

**Table 1.** Mass density, band gap energy, and refractive index of selected $TiO_2$ modifications.

| Modification | Mass Density gcm$^{-3}$ | Band Gap $E_g$ eV | $E_g/hc$ cm$^{-1}$ | $E_g/2hc$ cm$^{-1}$ | Refractive Index $n$@589 nm |
|---|---|---|---|---|---|
| anatase | 3.79–3.97 | 3.23 | 26,050 | 13,025 | 2.537 |
| brookite | 4.08–4.18 | 3.14 | 25,324 | 12,662 | 2.623 |
| rutile | 4.23 | 3.02 | 24,353 | 12,177 | 2.709 |
| PIAD $TiO_2$ film | ≈3.70 | 3.33 | 26,850 | 13,425 | 2.33 |
| IBS $TiO_2$ film [17,18] | 3.93 | 3.26 | 26,291 | 13,146 | 2.45 |

Note that, according to this model calculation, the main difference between the different modifications is in the onset energy of the TPA processes. The maximum $\beta$ value is residually influenced by the choice of the modification, because material modifications with a lower gap tend

to have a higher refractive index (compare Figure 2, where this trend is represented graphically for the sake of clarity), such that in Equation (1), the changes in $n$ and $E_g$ tend to cancel each other out. For reference purposes, we also include data from two thin-film samples, namely a sample produced by plasma ion-assisted evaporation (PIAD) as well as an ion beam-sputtered (IBS) sample, the latter prepared at Laser Zentrum Hannover LZH (for details, see Reference [17]). IBS is known as a preparation method that yields high-quality optical films with a rather high mass density. Indeed, the IBS data (Figure 2) fall closer to the values reported for the crystalline modifications than the PIAD sample does.

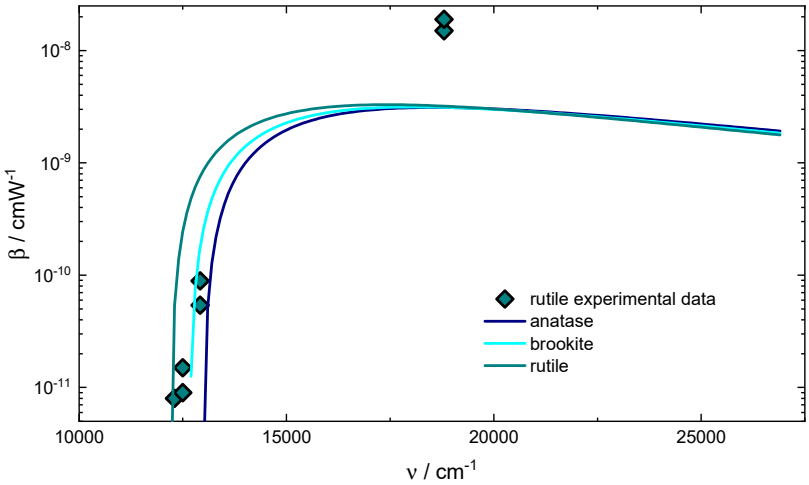


**Figure 1.** Two-photon absorption (TPA) coefficient as calculated from Equation (1) for crystalline $TiO_2$ modifications (solid lines; input data according to Table 1). Symbols: Experimental data reported in References [19,25] for rutile, as obtained from Z-scan techniques.

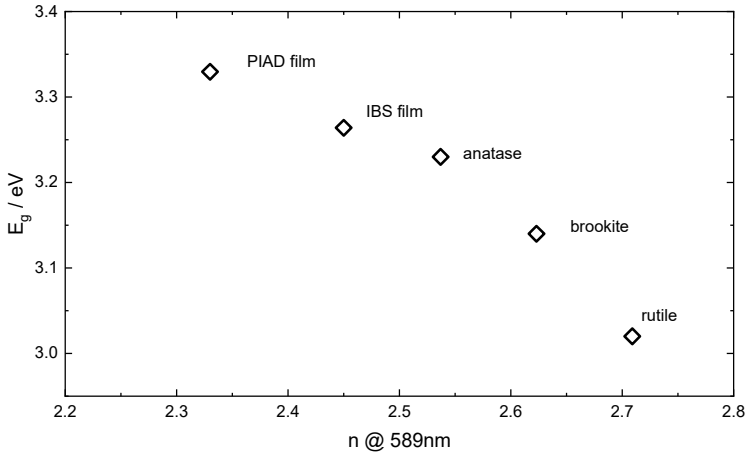


**Figure 2.** Correlation between optical gap and refractive index for the $TiO_2$ modifications from Table 1.

As previously mentioned, reported values for the nonlinear optical constants of $TiO_2$ are rare. Table 2 presents some published values of nonlinear refractive indices and absorption coefficients.

Note that the experimental β values published in Reference [25] are in rather good agreement with the theory (Figure 1), while those published in Reference [19] exceed the theoretically predicted values for a factor of approximately 5, such that experiment and theory indeed fall into the same order of magnitude anyway.

**Table 2.** Reported values for measured nonlinear $TiO_2$ optical constants. IAD denotes ion-assisted evaporation. C denotes the direction of the rutile optical axis, while E denotes the direction of the electric field vector in the light wave. IBS: Ion beam-sputtered.

| Sample | Source | $\nu$/cm$^{-1}$ | | $n_2$/cm$^2$ W$^{-1}$ | ß/cm W$^{-1}$ |
|---|---|---|---|---|---|
| Rutile single crystal | [19] | 18,800 | C‖E<br>C⊥E | $-1.07 \times 10^{-13}$<br>$-1.02 \times 10^{-13}$ | $\approx 1.9 \times 10^{-8}$<br>$\approx 1.5 \times 10^{-8}$ |
| Anatase polycrystalline waveguide | [20] | 6452 | | $1.03 \times 10^{-15}$<br>$1.82 \times 10^{-15}$ | -<br>- |
| Crystal | [21] | 9434 | | $\approx 9.4 \times 10^{-15}$ | - |
| IBS waveguide layer | [22] | 6452 | | $\approx 3 \times 10^{-14}$ | - |
| Rutile | [23] | 9434 | | $\approx 2 \times 10^{-14}$ | - |
| IAD thin film | [24] | 19,800 | | $\approx 3 \times 10^{-12}$ | - |
| Rutile | [25] | 12,300 | C‖E<br>C⊥E | -<br>- | $<1 \times 10^{-17}$<br>$8 \times 10^{-12}$ |
| | | 12,500 | C‖E<br>C⊥E | -<br>- | $9 \times 10^{-12}$<br>$1.5 \times 10^{-11}$ |
| | | 12,920 | C‖E<br>C⊥E | -<br>- | $8.9 \times 10^{-11}$<br>$5.4 \times 10^{-11}$ |
| $TiO_2$ thin film | [26] | 12,500 | | $7.9 \times 10^{-15}$ | - |

As a second approach, we will make use of the beta-distributed oscillator (ß_do) model [16]. This is a semiempirical model primarily developed for fitting linear optical constants, but again, all of the input parameters can be fitted from linear optical spectra. The dielectric function $\varepsilon$ in terms of the ß_do model is given by

$$\begin{array}{l} \varepsilon(\nu) = [n(\nu) + ik(\nu)]^2 = 1 + \frac{J}{\pi} \frac{\sum_{s=1}^{M} w_s \left( \frac{1}{\nu_s - \nu - i\Gamma} + \frac{1}{\nu_s + \nu + i\Gamma} \right)}{\sum_{s=1}^{M} w_s}; \\ w_s = \left( \frac{s}{M+1} \right)^{A-1} \left( \frac{M+1-s}{M+1} \right)^{B-1}; s = 1, 2, 3, \ldots, M; A, B > 0 \\ \nu_s = \nu_a + \frac{\nu_b - \nu_a}{M+1} s \end{array} , \quad (2)$$

while the real parameters $J$, $\Gamma$, $A$, $B$, $\nu_a$, and $\nu_b$ are free parameters within the ß_do model [16], and $M$ is the number of individual Lorentzian oscillators. Here, $n$ and $k$ are the linear refractive index and the extinction coefficient, correspondingly. Then, the third-order nonlinear susceptibility $\chi^{(3)}$ may be estimated by

$$\begin{array}{l} \chi^{(3)} \approx J_3 g(\nu) f(\nu)^2 \left( \sum_{s=1}^{M} w_s \right)^{-3}; \nu < \nu_a \\ f(\nu) = \sum_{s=1}^{M} w_s \left( \frac{1}{\nu_s - \nu - i\Gamma} + \frac{1}{\nu_s + \nu + i\Gamma} \right) \\ g(\nu) = \sum_{s=1}^{M} w_s \left( \frac{1}{\nu_s - 2\nu - i\Gamma} + \frac{1}{\nu_s + 2\nu + i\Gamma} \right) \end{array} , \quad (3)$$

which leads us to expressions for the nonlinear refractive index $n_2$ and the TPA coefficient β according to [27]

$$\begin{array}{l} n_2(\nu) = \frac{3}{4} \frac{\mu_0 c}{(n^2 + k^2)} \left[ \mathrm{Re}\chi^{(3)} + \frac{k}{n} \mathrm{Im}\chi^{(3)} \right] \\ \beta(\nu) = 3 \frac{\mu_0 \pi c \nu}{(n^2 + k^2)} \left[ \mathrm{Im}\chi^{(3)} - \frac{k}{n} \mathrm{Re}\chi^{(3)} \right] \end{array} , \quad (4)$$

in which $\mu_0$ represents the free space permeability. Note that the expressions written here are also valid in the case where there is still some linear absorption present in the TPA region [27]. In this approach, the parameter $J_3$ is estimated from the generalized millers rule according to References [14,16,28]. The gap values indicated in Table 1 for the PIAD and IBS samples correspond to $hcv_a$.

## 3. Experiment

### 3.1. PIAD Film Deposition

All samples were prepared in a Bühler Syrus LCIII deposition plant at Fraunhofer IOF using an electron-beam gun HPE6 and $Ti_3O_5$ as starter material. A target layer thickness of 200 nm was controlled by quartz crystal monitoring. For characterization, two different fused silica substrates (spectrophotometric characterization: Diameter 25 mm, thickness 1 mm; direct absorption measurement: Rectangular block $20 \times 20 \times 6$ mm$^3$) located in adjacent positions with identical radial positions in the rotating substrate holder, as well as silicon wafers, were used. During layer growth, additional energetic particle bombardment by means of a Bühler Advanced Plasma Source APS pro was accomplished. For this, two gas fluxes, $\Gamma_1$ and $\Gamma_2$ (for either argon or xenon as an inert gas), were used. In all experiments, the oxygen flow $\Gamma_3$ was 15 sccm, and the substrate temperature was around 110 °C. Additional main deposition parameters are summarized in Table 3.

**Table 3.** Main deposition parameters for the plasma ion-assisted evaporation (PIAD) preparation of the titanium dioxide single-layer coatings.

| Sample | r/nms$^{-1}$ | $U_B$/V | Inert Gas | $\Gamma_1$/sccm | $\Gamma_2$/sccm |
|---|---|---|---|---|---|
| 1 | 0.1 | 120 | Ar | 6 | 6 |
| 2 | 0.5 | 160 | Xe | 2 | 2 |
| 3 | 0.1 | 160 | | | |

### 3.2. Energy-Dispersive X-Ray Spectroscopy (EDX)

EDX measurements were performed using a high-resolution scanning electron microscope (FE-SEM Sigma, Carl Zeiss Microscopy GmbH, Oberkochen, Germany). Spectra were analyzed using INCA Software (INCA Energy 250, INCA Oxford Instruments GmbH, Wiesbaden, Germany). EDX measurements were performed with samples deposited onto silicon substrates. As the EDX method is not particularly surface-sensitive, the detection volume is dependent on the acceleration voltage and includes the film as well as parts of the substrate. In order to eliminate the substrate response, the film atomic composition was estimated from a combined elaboration of two EDX spectra obtained from different acceleration voltages (10 kV and 16 kV) for each sample.

### 3.3. Spectrophotometric Characterization

The transmittance ($T$) and reflectance ($R$) of all samples were measured in the spectral range of 320–2000 nm at near-normal incidence as well as at an incidence angle of 60° (in s- and p-polarization) in a Perkin Elmer Lambda 900 scanning spectrophotometer using the VN measurement technique [29]. From these spectra, film thickness $d$ as well as optical constants $n$ and $k$ were obtained as a result of spectra fits in terms of Equation (2) (using a Matlab environment). In all spectra fits, the number of individual Lorentzian oscillators $M$ in Equation (2) was set to $M = 10,000$, which has been proven to model a smooth function [16].

### 3.4. Direct Absorption Measurements

Light absorption measurements in $TiO_2$ films were measured directly using a laser-induced deflection (LID) technique [30,31]. This technique belongs to an ensemble of photothermal techniques with a pump–probe configuration. When the pump laser hits the sample under investigation,

the absorbed pump laser power forms a temperature profile (Figure 3, left). The latter is turned into a refractive index profile (=the thermal lens) by both the thermal expansion and the temperature-dependent refractive index. The refractive index gradient accounts for a deflection of the probe beams (from the same laser source) that is proportional to the absorbed pump laser power.

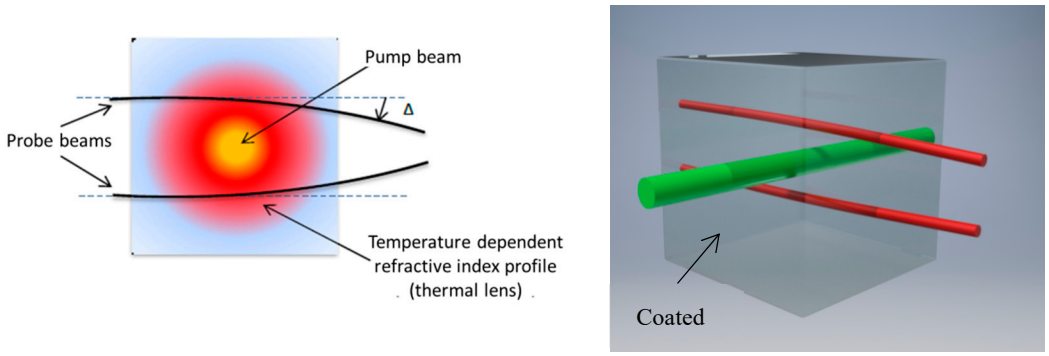


**Figure 3.** General scheme for the laser-induced deflection (LID) photothermal technique (**left**) and the measurement concept for rectangular substrate geometries (**right**).

Figure 3 (right) shows the applied measurement concept for the investigated rectangular substrate geometry ($20 \times 20 \times 6$ mm$^3$) with one coated surface. Two-probe beams above/beneath the irradiated spot utilize the probe beam deflection perpendicular to the pump beam direction. To measure coatings, the probe beams pass the sample close to the coated surface. In the case of transparent coatings, the probe beam deflection always comprises both the coating and substrate absorption. In order to distinguish both absorption contributions, an uncoated reference substrate of the same geometry/material is measured additionally, and the difference in the deflection signals is assigned to the coating absorption.

Calibration of the measurement setup is required to obtain absolute absorptance data from the deflection signals. For the LID technique, electrical calibration is applied, i.e., the thermal lens is generated by particular electric heaters. In the case of coating/surface absorption, small surface-mounted device (SMD) elements—fixed onto a very thin copper plate (thickness ~200 µm)—are placed centrally onto the surface of a reference substrate (of the same geometry and material) [32]. The copper plate allows for the required high thermal conduction to the sample. The validity of this calibration approach has been verified through separate measurements of reflectance, transmittance, absorptance, and scattering for different materials and coatings. The results of these energy balance measurements confirmed that in terms of measurement accuracy, a value of 1 was obtained in each of the investigations [33]. The calibration procedure itself is composed of measuring the probe beam deflection as a function of the electric power. Plotting the deflection signals versus electrical power (Figure 4) gives a linear function that spans several orders of magnitude for electric power, and the calibration coefficient $F_{CAL}$ is defined by the slope of the linear function (including the zero-point, i.e., no electrical power means no probe beam deflection) [31]. From the LID deflection signal $I_{LID}$ (for the sample under investigation), the corresponding mean pump laser power $P_L$, and the calibration coefficient $F_{CAL}$, the coating absorptance (defined as the ratio of the absorbed and incident light intensity) is calculated by

$$\text{absorptance} = \frac{I_{LID}}{F_{CAL} P_L}. \quad (5)$$

Laser irradiation at around 800 nm was realized by two different laser sources. For low-intensity measurements, an 808-nm continuous-wave semiconductor laser (HangZhou Naku Technology Co., Ltd.) with a maximum output power of 10 W was applied. The laser beam was shaped to a spatial profile of about $2 \times 2$ mm$^2$ on the sample. For elevated laser intensities in the GW/cm$^2$ range, an 800-nm Femtosecond laser (Astrella-V-F-1k, Coherent Inc.) with a pulse duration of 82 fs, a repetition rate of 1 kHz, and an average power of up to 2.1 W was used. In order to vary the laser intensity and maintain

the laser pulse duration, a combination of a thin-film polarizer and a polarizing beam splitter was placed into the beam path. A telescope was used to shape the Gaussian laser output beam to a $1/e^2$ Diameter of 5.4 mm on the sample under investigation.

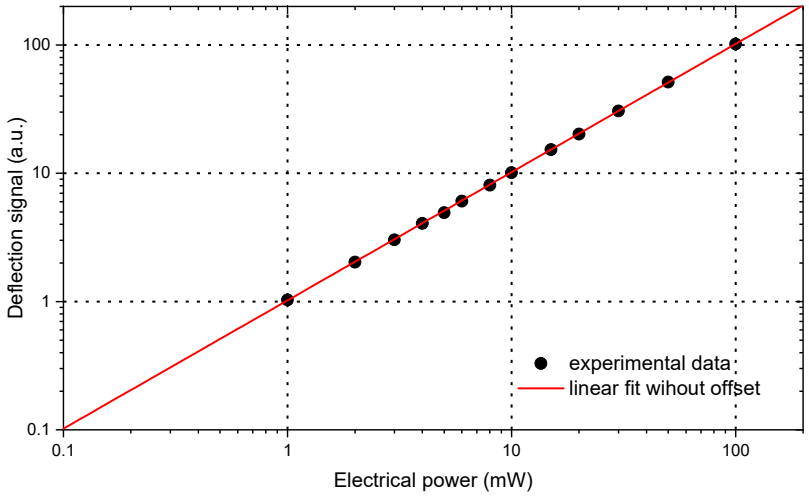


**Figure 4.** Measured deflection signal as a function of the electrical power (dots) and the linear fit without offset (red line) used for a determination of the calibration coefficient.

For a wavelength of 800 nm, the optical thickness of a 200-nm-thick $TiO_2$ film is not equal to λ/4 or multiples of λ/4. Therefore, laser beam reflection at the interface of the air/$TiO_2$ film was not negligible. The calculated reflectance amounts (up to about 15%) were taken into account for the determination of the average laser power $P_L$ inside the $TiO_2$ film.

## 4. Results

### *4.1. Linear Optical Constants from Spectrophotometry and Their Parametrization*

The linear optical constants of the titanium dioxide samples were fitted by means of Equation (2). In Figure 5, the measured and modeled transmittance and reflectance for sample 3 at near-normal incidence and at 60° for s- and p-polarization and the corresponding optical constants are shown. The complete set of calculated model parameters is summarized in Table 4.

**Table 4.** Here, beta-distributed oscillator (ß_do) parameters of all samples obtained from the spectra fitting.

| Sample | $M$ | $\nu_a$/cm$^{-1}$ | $\nu_b$/cm$^{-1}$ | Γ/cm$^{-1}$ | $A$ | $B$ | $J$/cm$^{-1}$ | $d$/nm | $J_3$/V$^{-2}$ cm$^5$ |
|---|---|---|---|---|---|---|---|---|---|
| 1 | 10,000 | 26,690 | 106,690 | 40 | 3.15 | 7.35 | 291,960 | 201.5 | 0.001679 |
| 2 | 10,000 | 26,975 | 106,792 | 40 | 3.14 | 7.32 | 287,543 | 194.6 | 0.001570 |
| 3 | 10,000 | 26,850 | 106,850 | 50 | 3.07 | 7.04 | 291,600 | 195.5 | 0.001654 |

In order to verify the film elementary composition, EDX measurements were performed. Uncorrected (raw) data on the elementary composition contained a significant substrate contribution, which increased with increasing acceleration voltage. In order to eliminate the substrate contribution, each sample was measured with two acceleration voltages, and the (corrected) elementary composition of the film was estimated using Equation (6):

$$\begin{aligned} N_{\text{corrected,Ti}} &= \frac{N_{\text{raw,Si,16}}N_{\text{raw,Ti,10}} - N_{\text{raw,Si,10}}N_{\text{raw,Ti,16}}}{N_{\text{raw,Si,16}} - N_{raw,\text{Si,10}}} \\ N_{\text{corrected,ng}} &= \frac{1}{2}\left[\frac{N_{\text{raw,ng,16}}}{N_{\text{raw,Ti,16}}} + \frac{N_{\text{raw,ng,10}}}{N_{\text{raw,Ti,10}}}\right]N_{\text{corrected,Ti}} \\ N_{\text{corrected,O}} &= 1 - N_{\text{corrected,Ti}} - N_{\text{corrected,ng}} \end{aligned} \quad . \tag{6}$$

Generally, *N* denotes the atomic concentration, whereas "raw" and "corrected" subscript indicate raw and corrected values, respectively. Accordingly, "10" or "16" subscripts indicate the raw values obtained at 10 and 16 kV of acceleration voltage, respectively. Here, ng stands for the noble gas used, i.e., argon or xenon.

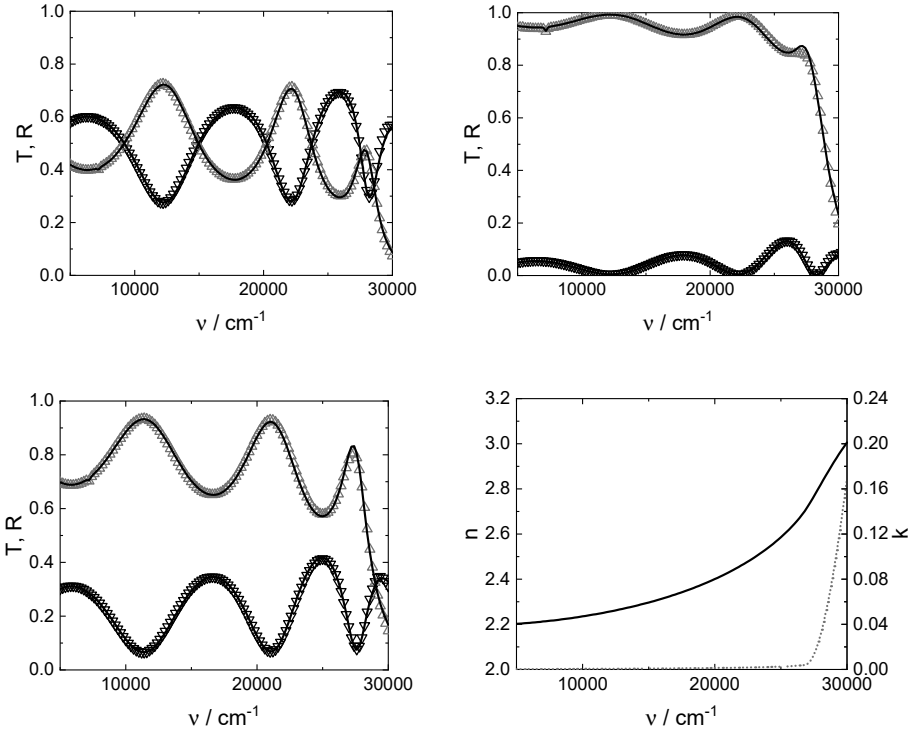


**Figure 5.** Modeled (solid line) and measured transmittance (up triangles) and reflectance (down triangles) at 60° for s- (**top left**) and p-polarizations (**top right**) and at near-normal incidence (**bottom left**) for sample 3 and modeled optical constants (**bottom right**, refractive index: Solid line, left axes; extinction coefficient: Dotted line, right axes).

The final calculated atomic concentrations are summarized in Table 5.

**Table 5.** Energy-dispersive X-ray spectroscopy (EDX) results and linear refractive index of the PIAD films.

| Sample | $N_{corrected,Ti}$ at % | $N_{corrected,O}$ at % | $N_{corrected,Ar}$ at % | $N_{corrected,Xe}$ at % | *n*@800 nm (12,500 $cm^{-1}$) |
|---|---|---|---|---|---|
| 1 | 32 | 64 | 4 | - | 2.269 |
| 2 | 31 | 66 | - | 3 | 2.253 |
| 3 | 32 | 65 | - | 3 | 2.261 |

Note that sample 1 had the highest refractive index, such that we expected the largest density for that sample. This was in agreement with the EDX results, indicating a correct stoichiometric relation between titanium and oxygen atoms. Samples 2 and 3 showed some more oxygen in the EDX analysis, indicating a somewhat porous layer structure with some incorporated water molecules. Correspondingly, the refractive index turned out to be smaller. Noble gas impurities from the used inert gas of the plasma source (Table 3) were of the order of 3 to 4 at % in all samples.

### *4.2. LID: Absorption Properties of the Films*

Figures 6–8 give the film absorptance as a function of the laser intensity for the three investigated $TiO_2$ films. Table 6 summarizes the linear absorptance and the TPA coefficients.

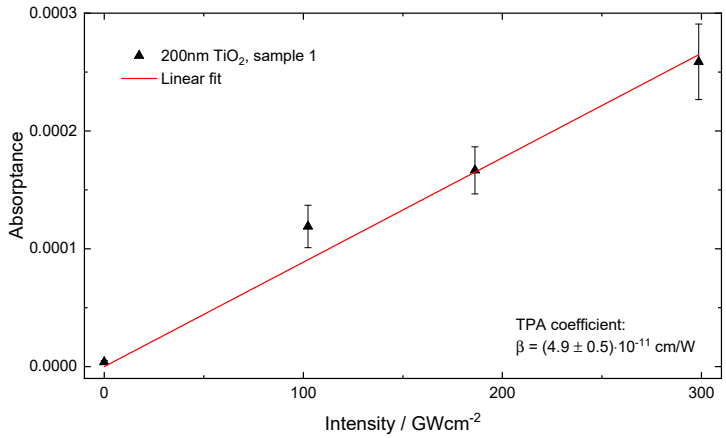


**Figure 6.** Absorptance versus laser intensity and the TPA coefficient for sample 1.

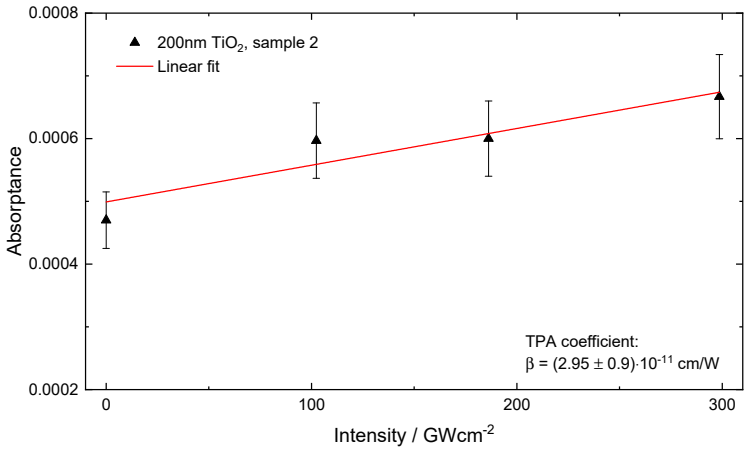


**Figure 7.** Absorptance versus laser intensity and the TPA coefficient for sample 2.

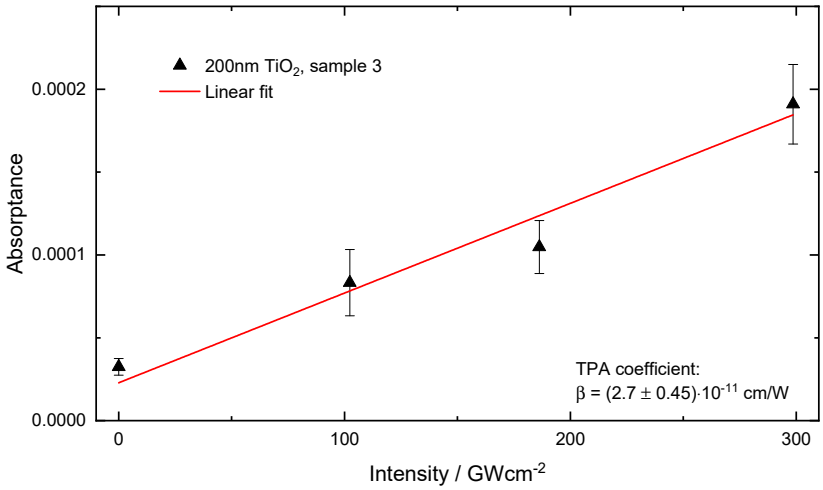


**Figure 8.** Absorptance versus laser intensity and the TPA coefficient for sample 3.

**Table 6.** LID results.

| $TiO_2$ Film | Linear Absorptance at 808 nm (ppm) | TPA Coefficient at 800 nm (12,500 $cm^{-1}$) ($10^{-11}$ cm/W) |
|---|---|---|
| 1 | (3.9 ± 1.3) | (4.9 ± 0.5) |
| 2 | (470 ± 50) | (3.0 ± 1.0) |
| 3 | (32 ± 6) | (2.7 ± 0.5) |

## 5. Discussion

### *5.1. Film Absorption*

Linear absorption in $TiO_2$ films at 800 nm has been shown to be as low as a few ppm, but varies over two orders of magnitude. No correlation was found between linear and nonlinear absorption properties. The observed TPA coefficients were less than one order of magnitude higher than previously published TPA coefficients in the range of 0.9–1.5 × $10^{-11}$ cm/W (measured at 800 nm in bulk rutile ($TiO_2$)) [25]. However, this finding is in agreement with earlier experimental results for fluoride thin films at 193 nm [34]. Here, it was demonstrated that the TPA coefficients of thin films were significantly larger than those obtained for the corresponding bulk materials.

On the other hand, the TPA coefficients observed in this study were about three orders of magnitude smaller than the values published in Reference [19] (compare Table 2), which was obviously a result of the different wavenumbers. Indeed, the photon energy in our study was still slightly below the value of $E_g/2$ (which we will further call the TPA threshold energy), while in Reference [19], the photon energy was well above that value. In order to visualize that, Figure 9 presents the measured TPA coefficients together with those calculated according to both the Sheik–Bahae (Equation (1), solid lines) and ß_do (dashed lines) models. Note that both models predicted an increase in β by almost three orders of magnitude when the wavenumber was changed from 12,500 to 18,800 $cm^{-1}$. This way, both models reproduced the dynamic range observed in the measured values. What is particularly remarkable is the good mutual agreement between both model approaches in the mentioned spectral region: The models delivered remarkably different results only when the photon energy came close to the single photon absorption edge at wavenumbers around 26,500 $cm^{-1}$. For reference purposes, we parametrized the dielectric function of the IBS sample specified in References [17,18] in terms of the ß_do model and included corresponding estimations of the TPA coefficient with Figure 9: Similarly to what is shown in Figure 1, the Sheik–Bahae model predicted a wavenumber shift of the spectral features without significant changes in the maximum absorption. On the contrary, note that in the ß_do model, the larger density of the IBS layer resulted in an increase in β, so that the calculated TPA coefficient came closer to the rutile value from Reference [19]. Again, for reference purposes, we included the rutile TPA simulation in terms of Equation (1) with Figure 9.

Note that the wavenumbers around 12,500 $cm^{-1}$ fell close to the TPA threshold wavenumbers in $TiO_2$. In the case of the rutile data from Reference [25], the Sheik–Bahae model (dark cyan line) provided a good theoretical reproduction of the TPA coefficients, because the excitation wavenumbers (Table 2) were still higher than the corresponding TPA threshold wavenumber (12,177 $cm^{-1}$, compare Table 1), which was required for calculation in terms of Equation (1). However, the measured PIAD data could not be reproduced in terms of the Sheik–Bahae model (solid black line) with the parameters given in Table 1. The reason is that in Equation (1), the excitation wavenumber should exceed the TPA threshold, which corresponds to 13,345–13,490 $cm^{-1}$ for the PIAD samples (Tables 1 and 4). This was not achieved in our measurements. Clearly, the PIAD films were essentially amorphous, such that the optical gap (and correspondingly the TPA thresholds) did not represent "hard" threshold energies. Instead, band tailing allowed for absorption even when the photon energy was smaller than the corresponding "threshold". Note that in this connection, the ß_do model predicted a certain TPA even below the thresholds, which turned out to be less than one order of magnitude smaller than the measured absorption. Clearly, films produced by evaporation are usually highly defective and maybe

somewhat contaminated, and it is therefore not so surprising that the measured absorption values somewhat exceeded the modeled ones.

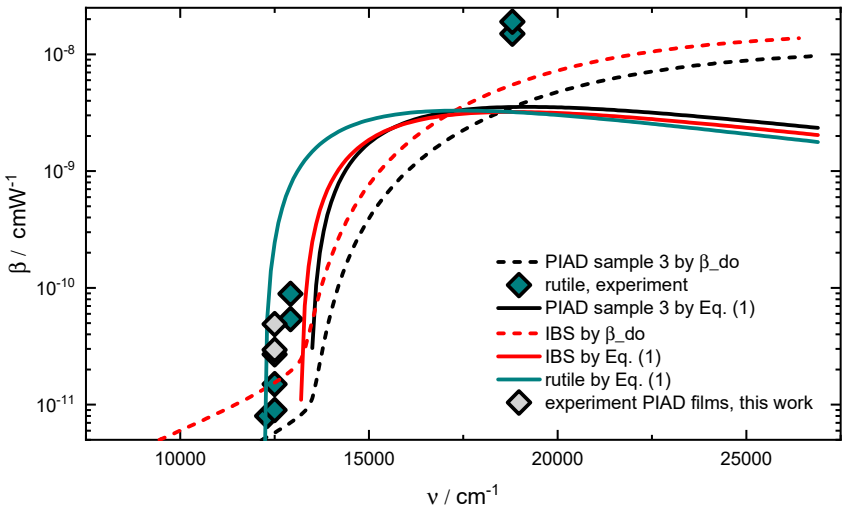


**Figure 9.** Measured TPA coefficients from rutile and PIAD $TiO_2$ compared to simulations in terms of Equations (1), (3), and (4).

### *5.2. Considerations Regarding Nonlinear Refraction*

It should be mentioned that both model approaches allowed for estimating the nonlinear refractive index as well, and such like calculations could be compared to the reported experimental data collected in Table 2. This is shown in Figure 10 (excluding the extraordinarily large value from Reference [24]). The predictions of the Sheik–Bahae model (assuming the input data from Table 1) almost coincided with the chosen ordinate scaling and were in reasonable agreement with the experimental data from References [20–23,26]. The ß_do model delivered results in the infrared that practically coincided with the Sheik–Bahae model predictions up to the TPA threshold. At higher wavenumbers, both approaches delivered divergent results. Note that none of the models was able to reproduce the strongly negative $n_2$ value from Reference [19], but the Sheik–Bahae model came at least close to this value. This is not astonishing, because in the ß_do approach (Equations (3) and (4)), only the TPA resonant contribution to $n_2$ is taken into account, while nonresonant contributions are not considered at all.

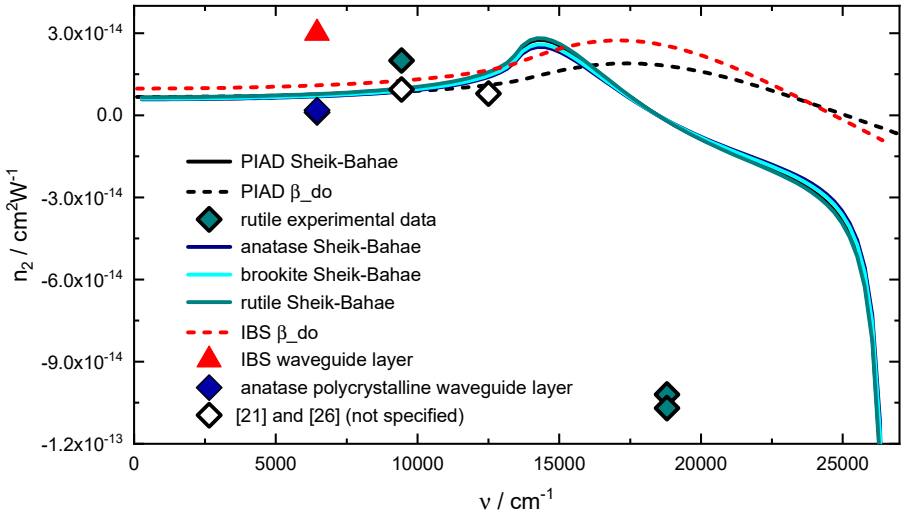


**Figure 10.** Measured nonlinear refractive indices from different $TiO_2$ modifications compared to simulations in terms of the Sheik–Bahae approach as well as Equations (3) and (4).

The relative stability of the Sheik–Bahae approach with respect to correlated changes in the optical gap and the refractive index makes it difficult to understand density-related differences in the nonlinear response of different $TiO_2$ modifications. Nevertheless, a density dependence of $n_2$ and β is physically reasonable and expected. It seems to be an advantage of the ß_do model that differences in the density are explicitly taken into account in terms of the model parameter $J$; consequently, the modeled $n_2$ data for the IBS film is larger than those of the PIAD film. This way, the ß_do model might provide access to explaining the significant scatter in measured nonlinear constants, as has been reported in the different studies cited. For future practical modeling, it might therefore be useful to merge both models in a suitable way.

### *5.3. Considerations Regarding the Effect of the Nonlinear Film Properties on Elastic Scattering*

Albeit not the main scope of this paper, we would like to briefly consider the role of light scattering and the potential impact of nonlinear effects on light scattering properties. We focus here on elastic scattering processes, because with conventional laser coatings, elastic scattering is four orders of magnitude stronger than inelastic scattering. Nevertheless, one must keep in mind that the excitation of nonlinear optical processes may also result in an increase in inelastic scatter contributions, but this discussion is outside the scope of this paper.

For most interference coatings, the interface roughness is the dominating source of light scattering. The angle-resolved scattering (ARS) can be calculated using multilayer vector perturbation (VPT) theories (given in detail, for instance, in References [35–37] and summarized briefly in Reference [38]). The most relevant factors influencing light scattering properties are (i) interface roughness, (ii) the cross-correlation properties of the roughness of different interfaces, (iii) the field strengths at the interfaces, and (iv) the interference properties not only for the specular fields but also for the scattered fields (the latter of course being linked to wavelengths and incident angles). Defects and contamination on the coatings can be considered to be additional sources of light scattering, which we excluded from this discussion.

As a result of VPT, the angle-resolved scattering distribution (the scattered intensity) of a multilayer can be calculated as

$$ARS(\theta_s) = \frac{16\pi^2}{\lambda^4} \sum_{i=0}^{Z} \sum_{j=0}^{Z} F_i F_j^* PSD_{ij}(f), \tag{7}$$

where $Z$ is the number of layers (of course $Z = 1$ for a single film), and $F_i$ and $F_j$ are optical factors containing information about the optical properties of the perfectly smooth multilayer (design, dielectric functions, etc.) and the conditions of illumination and detection (angles, polarization, etc.). The roughness factor $PSD_{ij}$ comprises the power spectral density functions of all interfaces (for $i = j$) and their cross-correlation properties (for $i \neq j$). The total scatter can be calculated by integrating Equation (7).

It is important to go back into the full treatment of the VPTs to assess the influence of nonlinear effects. The main approach of VPT is that the unperturbed specular fields are used to calculate the fields at the interfaces. Depending on the roughness structure, these fields drive surface currents, which produce scattered waves. These scattered waves then propagate through the coating and interfere. Therefore, we expect an influence of nonlinear effects on the scattering properties in two ways: (i) the field-induced change of the dielectric function leads to a modification of the field distribution inside the coating and hence modified fields at the interfaces, and (ii) the modified dielectric properties change the propagation and interference properties of the scattered waves. It has been demonstrated that even small changes in the field distribution, e.g., caused by small wavelength shifts, can easily lead to an enhancement of the scatter losses by an order of magnitude [38]. Simply put, if for whatever reason the observed specular field deviates from the expected values by several percentage points, a substantial change in the scatter losses can be expected.

Although not trivial, we believe that taking nonlinear effects into account in scatter modeling is straightforward. One precondition is that the scattering effects are still so weak that they do not influence the determination of the dielectric function, including nonlinear effects using the approaches described in this paper. We should then be able to use these new parameters to calculate the scattered fields. Further studies will show if this pragmatic approach is justified. We also believe that for interference coatings, once we have taken nonlinear effects into account in the design, we are also able to bring the light scattering properties back to the level we would expect for a similar coating designed for low fluences, or we even have the possibility of making use of nonlinear effects for scatter loss reduction.

## 6. Conclusions

We presented experimental results on the optical properties of PIAD titanium dioxide thin films, with a focus on their absorption behavior. In addition to a rather conventional linear optical characterization, TPA coefficients at a wavelength of 800 nm were obtained from laser-induced deflection measurements and were compared to the values reported so far for rutile crystals in terms of a Z-scan technique. It turns out that the TPA coefficients obtained from our LID measurements were very consistent with what has been reported in the literature in terms of manageable models describing the TPA coefficient, such as the Sheik–Bahae model and the ß_do approach.

We provided a further discussion on the accompanying changes in the refractive index in terms of nonlinear refraction and discussed their possible impact on the elastic light scattering characteristics of dielectric coatings at high light intensities.

**Author Contributions:** Conceptualization, O.S.; formal analysis, O.S., S.W., S.S., and C.M.; funding acquisition, S.W.; methodology, O.S., S.W., and C.M.; project administration, S.W.; software, S.W.; validation, O.S., S.W., S.S., and C.M.; writing—Original draft, O.S.; writing—Review and editing, O.S., S.W., S.S., and C.M. All authors have read and agreed to the published version of the manuscript.

**Funding:** This research was funded by the Bundesministerium für Bildung und Forschung, grant number 13N10459, and by the European Regional Development Fund, grant number 2016 FE 9045.

**Acknowledgments:** The authors are grateful to Tina Seifert (Fraunhofer IOF) for performing the EDX measurements. We also thank Tsvetanka Babeva for the invitation to submit this study to a special issue of "Coatings" as a feature paper.

**Conflicts of Interest:** The authors declare no conflicts of interest. The funders had no role in the design of the study; in the collection, analyses, or interpretation of data; in the writing of the manuscript; or in the decision to publish the results.

## References

1. Born, M.; Wolf, E. *Principles of Optics*; Pergamon Press: Oxford, UK, 1968.
2. Furman, S.A.; Tikhonravov, A.V. *Basics of Optics of Multilayer Systems*; Editions Frontières: Paris, France, 1992.
3. Stenzel, O. *The Physics of Thin Film Optical Spectra: An Introduction*, 2nd ed.; Springer: Berlin, Germany, 2016.
4. Macleod, H.A. *Thin-Film Optical Filters*, 4th ed.; CRC Press: Boca Raton, FL, USA, 2010.
5. Thelen, A. *Design of Optical Interference Coatings*; McGraw-Hill: New York, NY, USA, 1989.
6. Shen, Y.R. *The Principles of Nonlinear Optics*; John Wiley & Sons Ltd.: Hoboken, NJ, USA, 1984.
7. Mourou, G.; Mironov, S.; Khazanov, E.; Sergeev, A. Single cycle thin film compressor opening the door to Zeptosecond-Exawatt physics. *Eur. Phys. J. Spec. Top.* **2014**, *223*, 1181–1188. [CrossRef]
8. Razskazovskaya, O.; Luu, T.T.; Trubetskov, M.; Goulielmakis, E.; Pervak, V. Nonlinear Behavior and Damage of Dispersive Multilayer Optical Coatings Induced by Two-Photon Absorption. *Proc. SPIE* **2014**, *9237*, 92370L1–92370L8.
9. Amotchkina, T.; Trubetskov, M.; Fedulova, E.; Fritsch, K.; Pronin, O.; Krausz, F.; Pervak, V. Characterization of Nonlinear Effects in Edge Filters. In Proceedings of the Optical Interference Coatings (OIC), Tucson, AZ, USA, 19–24 June 2016. Paper ThD.3.
10. Stenzel, O.; Wilbrandt, S. Theoretical study of multilayer coating reflection taking into account third-order optical nonlinearities. *Appl. Opt.* **2018**, *57*, 8640–8647. [CrossRef] [PubMed]

11. Tichá, H.; Tichý, L. Semiempirical relation between non-linear susceptibility (refractive index), linear refractive index and optical gap and its application to amorphous chalcogenides. *J. Optoelectron. Adv. Mater.* **2002**, *4*, 381–386.
12. Fournier, J.; Snitzer, E. The nonlinear refractive index of glass. *IEEE J. Quantum Electron.* **1974**, *10*, 473–475. [CrossRef]
13. Boling, N.L.; Glass, A.J.; Owyoung, A. Empirical Relationships for Predicting Nonlinear Refractive Index Changes in Optical Solids. *IEEE J. Quantum Electron.* **1968**, *14*, 601–608. [CrossRef]
14. Stenzel, O. Simplified expression for estimating the nonlinear refractive index of typical optical coating materials. *Appl. Opt.* **2017**, *56*, C21–C23. [CrossRef]
15. Sheik-Bahae, M.; Hutchings, D.C.; Hagan, D.J.; Van Stryland, E.W. Dispersion of Bound Electronic Nonlinear Refraction in Solids. *IEEE J. Quantum Electron.* **1991**, *27*, 1296–1309. [CrossRef]
16. Stenzel, O.; Wilbrandt, S. Beta-distributed oscillator model as an empirical extension to the Lorentzian oscillator model: Physical interpretation of the β_do model parameters. *Appl. Opt.* **2019**, *58*, 9318–9325. [CrossRef]
17. Stenzel, O.; Wilbrandt, S.; Kaiser, N.; Schmitz, C.; Turowski, M.; Ristau, D.; Awakowicz, P.; Brinkmann, R.P.; Musch, T.; Rolfes, I.; et al. Plasma and optical thin film technologies. *Proc. SPIE* **2011**, *8168*, 81680L.
18. Landmann, M.; Köhler, T.; Köppen, S.; Rauls, E.; Frauenheim, T.; Schmidt, W.G. Fingerprints of order and disorder in the electronic and optical properties of crystalline and amorphous $TiO_2$. *Phys. Rev. B* **2012**, *86*, 064201. [CrossRef]
19. Watanabe, Y.; Ohnishi, M.; Tsuchiya, T. Measurement of nonlinear absorption and refraction in titanium dioxide single crystal by using a phase distortion method. *Appl. Phys. Lett.* **1995**, *66*, 3431–3432. [CrossRef]
20. Shtyrkova, K. Characterization of Third Order Nonlinearities in $TiO_2$ Waveguides at 1550 nm. Master's Thesis, Massachusetts Institute of Technology, Cambridge, MA, USA, 2013.
21. Adair, R.; Chase, L.L.; Payne, S.A. Nonlinear refractive index of optical crystals. *Phys. Rev. B* **1989**, *39*, 3337–3350. [CrossRef]
22. Guan, X.; Hu, H.; Oxenløwe, L.K.; Frandsen, L.H. Compact titanium dioxide waveguides with high nonlinearity at telecommunication wavelengths. *Opt. Express* **2018**, *26*, 1055–1063. [CrossRef] [PubMed]
23. Friberg, S.R.; Smith, P.W. Nonlinear Optical Glasses for Ultrafast Optical Switches. *IEEE J. Quantum Electron.* **1987**, *23*, 2089–2094. [CrossRef]
24. Rigneault, H.; Flory, F.; Monneret, S. Nonlinear totally reflecting prism coupler: Thermomechanic effects and intensity-dependent refractive index of thin films. *Appl. Opt.* **1995**, *34*, 4358–4369. [CrossRef] [PubMed]
25. Evans, C.C.; Bradley, J.D.B.; Martí-Panameño, E.A.; Mazur, E. Mixed two- and three-photon absorption in bulk rutile ($TiO_2$) around 800 nm. *Opt. Exp.* **2012**, *20*, 3118–3128. [CrossRef]
26. Evans, C.C.; Bradley, J.D.B.; Parsy, F.; Phillips, K.C.; Senaratne, R.; Martí-Panameño, E.A.; Mazur, E. Thermally managed Z-scan measurements of titanium dioxide thin films. presented at Photonics West, San Francisco, CA, USA, 27 January 2011.
27. del Coso, R.; Solis, J. Relation between nonlinear refractive index and third-order susceptibility in absorbing media. *J. Opt. Soc. Am. B* **2004**, *21*, 640–644. [CrossRef]
28. Wang, C.C. Empirical Relation between the Linear and the third-order Nonlinear Optical Susceptibilities. *Phys. Rev. B* **1970**, *2*, 2045–2048. [CrossRef]
29. Stenzel, O. *Optical Coatings: Material Aspects in Theory and Practice*; Springer: Berlin, Germany, 2014; pp. 117–127.
30. Guntau, M.; Triebel, W. A Novel method to measure bulk absorption in optically transparent materials. *Rev. Sci. Instr.* **2000**, *71*, 2279–2282. [CrossRef]
31. Bublitz, S.; Mühlig, C. Absolute Absorption Measurements in Optical Coatings by Laser Induced Deflection. *Coatings* **2019**, *9*, 473. [CrossRef]
32. Mühlig, C.; Triebel, W.; Kufert, S.; Bublitz, S. Characterization of low losses in optical thin films and materials. *Appl. Opt.* **2008**, *47*, C135–C142. [CrossRef] [PubMed]
33. Mühlig, C.; Bublitz, S. Sensitive and absolute absorption measurements in optical materials and coatings by laser induced deflection (LID) technique. *Opt. Eng.* **2012**, *51*, 121812. [CrossRef]
34. Mühlig, C.; Bublitz, S.; Kufert, S. Nonlinear absorption in single $LaF_3$ and $MgF_2$ layers at 193 nm measured by surface sensitive laser induced deflection technique. *Appl. Opt.* **2009**, *48*, 6781–6787. [CrossRef] [PubMed]

35. Elson, J.; Rahn, J.; Bennett, J. Light scattering from multilayer optics: Comparison of theory and experiment. *Appl. Opt.* **1980**, *19*, 669–679. [CrossRef]
36. Bousquet, P.; Flory, F.; Roche, P. Scattering from multilayer thin films: Theory and experiment. *J. Opt. Soc. Am.* **1981**, *71*, 1115–1123. [CrossRef]
37. Amra, C.; Grezes-Besset, C.; Roche, P.; Pelletier, E. Description of a scattering apparatus: Application to the problems of characterization of opaque surfaces. *Appl. Opt.* **1989**, *28*, 2723–2730. [CrossRef]
38. Schröder, S.; Trost, M.; Herffurth, T.; von Finck, A.; Duparré, A. Light scattering of interference coatings from the IR to the EUV spectral regions. *Adv. Opt. Technol.* **2013**, *3*, 113–120. [CrossRef]